RESEARCH PAPER

Optimization of Parameters for the Friction Stir Processing and Welding of AA1050 Aluminum Alloy

Mahdi Alishavandi[1], Mahnam Ebadi[2], Amir Hossein Kokabi[1]*

* *kokabi@sharif.edu*
[1*] Department of Materials Science and Engineering, Sharif University of Technology, Tehran, Iran;
[2] Department of Materials Science and Engineering, Shiraz University, Shiraz, Iran

Received: October 2020 **Revised: January 2021** **Accepted: February 2021**
DOI: 10.22068/ijmse.2016

Abstract: *Friction-Stir Processing (FSP) was applied on AA1050 Aluminum Alloy (AA) to find the highest mechanical properties among 28 combinations of the rotational and traverse speed (800-2000 rpm and 50-200 mm.min^{-1}) and four different tool probe shapes (threaded, columnar, square and triangle). To this aim, the AA standard sheet went through a single pass of FSP. The 1600 rpm and 100 mm.min^{-1} with threaded tool probe was chosen as the best combination of rotational and traverse speed. Grain size at the Stirred Zone (SZ) was studied using Optical Microscopy (OM). The results showed that the SZ's grain size was refined from 30 µm down to about 12 µm due to dynamic recrystallization during FSP. The processed sample exhibited improved hardness, yield stress, ultimate tensile strength, elongation up to 65, 80, 66, and 14%, respectively, compared to the annealed AA sample. Studying fractographic features by OM and field emission scanning electron microscope (FESEM) revealed a dominantly ductile fracture behavior.*

Keywords: *Friction stir processing, AA1050 aluminum alloy, Tool probe shape, Grain structure, Mechanical properties, Rotational and traverse speed.*

1. INTRODUCTION

Aluminum Alloys (AA) are widely used in various industries such as automotive, aerospace, and most electronic portable devices [1–3]. The AAs are well-known metals due to high specific strength, corrosion resistance, and excellent formability [4]. During recent years there has been much effort to enhance the mechanical properties of AA sheets and joints [5]. Hall-Petch strengthening is an essential and fundamental method to enhance mechanical properties [6]. Severe Plastic Deformation (SPD) processes such as equal channel angular pressure, high-pressure torsion, accumulative roll bonding, and constrained groove pressing have been used for years to attain Ultra-Fine-Grained (UFG) structures and enhance the mechanical properties of these alloys [7, 8]. Friction Stir Processing (FSP) is an SPD technique and Thermo-Mechanical Process (TMP) developed by Mishra et al. [9] based on Friction Stir Welding (FSW). FSP is a solid-state process that consists of a tool inserted into the Base Metal (BM) and rotates; then, it makes frictional heat and pin's flow effect, a homogenous and refined structure is achieved [10]. Casting and surface modification are some other features of FSP, as well [1, 11]. The final microstructure and attained mechanical properties chiefly depend on Dynamic Recrystallization (DRX) and related annealing phenomena [12].

Recrystallization (RX) is defined by forming a new grain structure in a deformed material by the generation and migration of High Angle Grain Boundaries (HAGB) driven by the stored energy, which is achieved by plastic deformation [13]. There are two main types of RX, static and dynamic, which occur during annealing and high-temperature deformation, respectively [14]. The main factors with significant effects on DRX are Stacking Fault Energy (SFE), TMP conditions, initial grain size, chemical composition, solute elements, and Strengthening Particles (SP) [13, 15–18]. Three DRX phenomena are reported; Discontinuous Dynamic Recrystallization (DDRX) is often observed in low SFE materials. DDRX happens when the nucleation of strain-free grains is growing at the expense of grains full of dislocation [19]. Continuous Dynamic Recrystallization (CDRX) is seen in high SFE materials when cells or sub-grain structures are created with Low Angle Grain Boundaries (LAGB) during deformation; then, with further deformation, LAGB changes into HAGB [20–

22]. Geometric Dynamic Recrystallization (GDRX) is reported in AA, which undergoes considerable strain at high temperatures [12, 13, 19, 23] . In the Stir Zone (SZ), due to high temperature up to 0.9 melting point (T_m) and SPD, DRX phenomena are responsible for grain refinement. It is shown that in AA, 80% of grains in SZ have the HAGB character and 20% of grains have the LAGB character [24].

Various researchers successfully used different FSP parameters to improve the microstructural and mechanical properties of AA and revealed that optimum process parameters are described as ω =1000 rpm and ν=30 mm.min^{-1}. Mahmoud et al. [25] studied the influences of various rotational speed (ω), traverse speed (ν), and passes on A390 hypereutectic Al-Si as-cast alloy. The microstructural and mechanical improvement is achieved by removing cast defects; moreover, by increasing pass number, reducing ω , and increasing ν, the Si particulate size decreased. Pasebani et al. [26] showed that the constituent particles reduced substantially in FSPed wrought AA2024 by increasing ω from 200 to 1000 rpm and tensile properties enhanced. Vignesh et al. [27] studied the effect of different ω , ν, and tool shoulder diameters to improve wear resistance of AA5083. In all parameter combinations of FSPed samples, refined microstructure, increased hardness value, and increased wear resistance are reported.

FSP and FSW have a lot of similar concepts and parameters for materials modification and joining [28, 29]. These processes have the potential to remove cast defects and metal forming effects like drawing. Hence, by understanding and employing grain refinement and the DRX concept in FSP and FSW, a regular and inexpensive route to achieve one's desired properties, it is possible to find maximum grain refinement and the highest mechanical properties. Tool geometry has essential influences on FSP and FSW as it affects material flow, heat generation, and microstructure evolution. Also, tool material characteristics have a crucial role in FSP and should satisfy some requirements like machinability, cost, low coefficient of thermal expansion between probe and shoulder, high compressive yield strength at elevated temperatures, and low wear rate [1].

Today industries need to achieve higher strength AAs, increase indentation hardness value (HV), elongation percent (El%, ε%), and ultimate tensile strength (UTS), just by a straightforward method without adding any reinforcement particles, precipitation, or buying expensive grades of materials to save energy and time. To the best of our knowledge, the exact and precise combination of ν and ω along with the best tool probe shape for achieving the highest possible mechanical properties in FSPed and FSWed AA1050 have not been reported in the literature; therefore, we decided to evaluate these parameters in order to reduce the macrostructural and microstructural defects and achieve higher tensile properties in FSP and FSW. At last, FSPed samples were compared based on mechanical properties such as UTS, ε%, yield stress, and fracture stress. The highest mechanical properties among these samples can be utilized for AA joining by FSW and modification by FSP.

2. EXPERIMENTAL PROCEDURES

Initial specimens with dimensions of 210×70×4 mm^3 were cut from an AA1050-H14 sheet where chemical compositions, summarized in Table 1.

In order to remove the work hardening effects of rolling and transform elongated grains to equiaxed grains, specimens were annealed for 90 min at 427 °C. Different fixed tool probe shapes have been used in this research. Four different tool probes shown in Figure 1 were all utilized with a flat cylindrical end shape outer surface. All shoulders have a cylindrical outer surface, flat, and featureless end surface. The first one is square, or parallelogram end surface (Fig.1.a); the second one is triangle end surface (Fig.1.b), the third and fourth ones are a threaded cylinder outer surface with a circle-end surface and a smooth cylinder outer surface with a circular-end surface (Fig.1.c,d) respectively. The fixed tool probe dimensions are 18, 3.5, and 5 mm for shoulder, pin's length, and pin's diameter, respectively, with an apparatus tilt angle of 3°. The tool was made of H13 steel and heat-treated to increase Rockwell C (RC) hardness from 20 to 54 RC. Different combinations of ω from 800 to 2000 rpm and ν from 50 to 200 mm.min^{-1} have been used for FSP by threaded cylinder outer surface. The specimen with the highest tensile properties has been chosen to be FSPed by a different fixed tool probe. The cross-section of FSPed specimens

Table 1. Chemical composition of the AA1050 aluminum alloy (wt%).

Element	Al	Cu	Mg	Si	Fe	Mn	Zn	Ti	V
AA1050 Examined	Balanced	0.002	0.002	0.1	0.368	0.001	0.007	0.008	0.005
AA1050 ASTM	Balanced	<0.05	<0.05	<0.25	<0.4	<0.05	<0.05	<0.03	<0.05

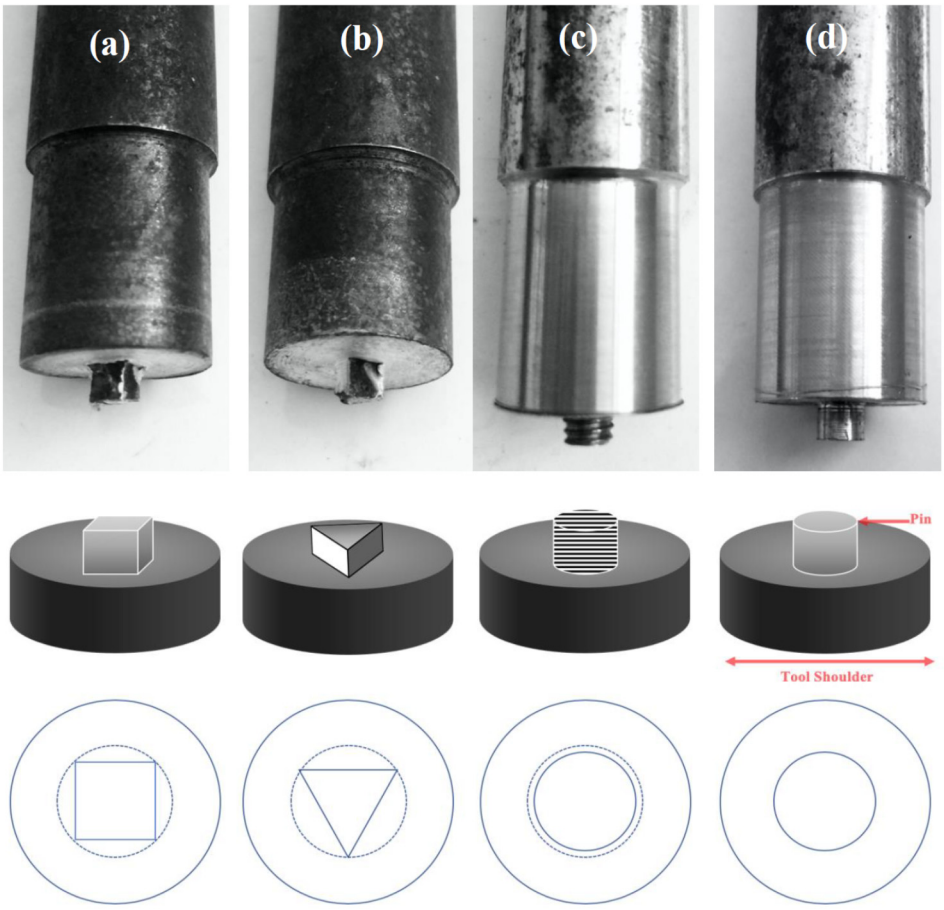

Fig. 1. Different tool probe shape: (a) square, (b) triangular, (c) threaded, (d) columnar.

was selected for further studies. The samples went through the standard metallographic procedures with SiC grinding papers (200-5000), mechanical polishing with 1-micron polycrystalline diamond suspension, electro-etching by 100 ml of H_2O, and 3 ml HBF_4 at the voltage of 20 V for 90-120 s. Optical microscopy (OM, Olympus PME3, Germany) and a stereographic (Nikon, USA) with polarized light were used to study the microstructural evolution after FSP. Mechanical properties like the uniaxial tensile test (Hounsfield H10KS) were evaluated according to ASTM E8M standard method at a constant cross-head speed of 1 mm/min under an ambient atmosphere and a constant strain rate of 6×10^{-4} sec^{-1}. Vickers micro-hardness (Buehler) test with a load of 500 gF and dwell time of 20 s at room temperature were carried out. For each condition, tests were repeated 3 times, and the average values were measured. To study the fracture surface in detail and reveal the mode of fracture, a Field-Emission Scanning Electron Microscope (FESEM) was used.

3. RESULTS AND DISCUSSION

3.1. Microstructural evolution in different heat input

The heat input (Q) in FSP relates directly to ω and inversely to ν which is illustrated in Figure 2 by the ratio of ω /ν (an index of different heat input for the combination of ν and ω). The Optical micrograph of the SZ microstructure with the highest mechanical properties, which is reported in section 3.3, for each ω and threaded cylinder outer surface with the circle-end surface is shown in Figure 3. In 28 combinations of ν and ω , a defect-free processed zone was achieved. The average grain size of annealed BM is 30 μm with relatively large equiaxed grains.

After applying a single FSP pass, microstructural refinement happened, and the smallest average grain size of 12 μm among 28 combinations was achieved, measured by ImageJ. The average grain size decreases with increasing ω , then increases by rising the Q or ω .

Microstructure refinement happened in all 28 combinations, which led to improved mechanical properties; moreover, the minimum possible average grain size was achieved. During FSP of AA, SPD occurs, shattering and smashing the grains and raising SZ's temperature near the AA's melting point and is favorable for DDRX, which is responsible for grain refinement in AA. DDRX mainly begins with bulging of the grain boundaries and forming a necklace structure of equiaxed recrystallized grains. Among the factors that affect DRX, like initial grain size, SP, and SFE; SFE is predominant and impacts DRX kinetics and AA's structure [30]. In the absence of SP in SZ, the particle-stimulated nucleation does not affect the final structure [31].

3.2. Microstructural features of different fixed tool probe shapes

After studying the microstructure of selected ω - ν combinations and finding the sample with highest mechanical properties (threaded pin shape, ω =1600 rpm, ν=100 mm.min^{-1}) among 28 combinations, new samples were used to be FSPed with 3 different pin shape to be compared with the threaded pin. As Figure 4 illustrates, all four probe shapes produce a defectless SZ; moreover, all samples have three distinct FSP standard zones: SZ, thermo-mechanical affected zone (TMAZ), and BM. In this study, HAZ was not observed because the AA had been annealed; therefore, the heat generated during FSP could not affect the BM grain size. Due to an insufficient strain in TMAZ, the grains have elongated shapes. There are no recrystallized or equiaxed grains in the TMAZ since DRX did not happen, and insufficient deformation could elongate grain [32, 33].

It was mentioned before that besides ν and ω , tool probe shape also impacts the material flow at elevated temperatures in FSP and microstructure. Heat generation and flow of plasticized material depend on different FSP variables, such as probe features. Each probe has distinguishable

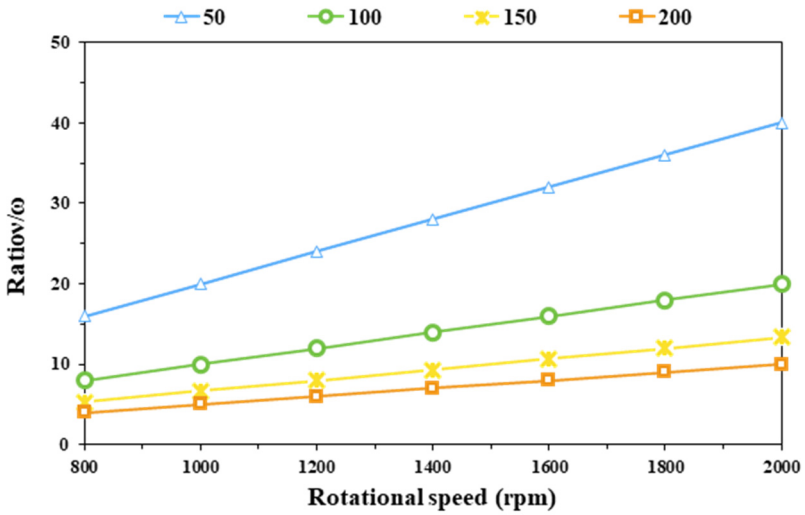

Fig. 2. ω/v ratio (as an indicator of heat input) for 28 combinations.

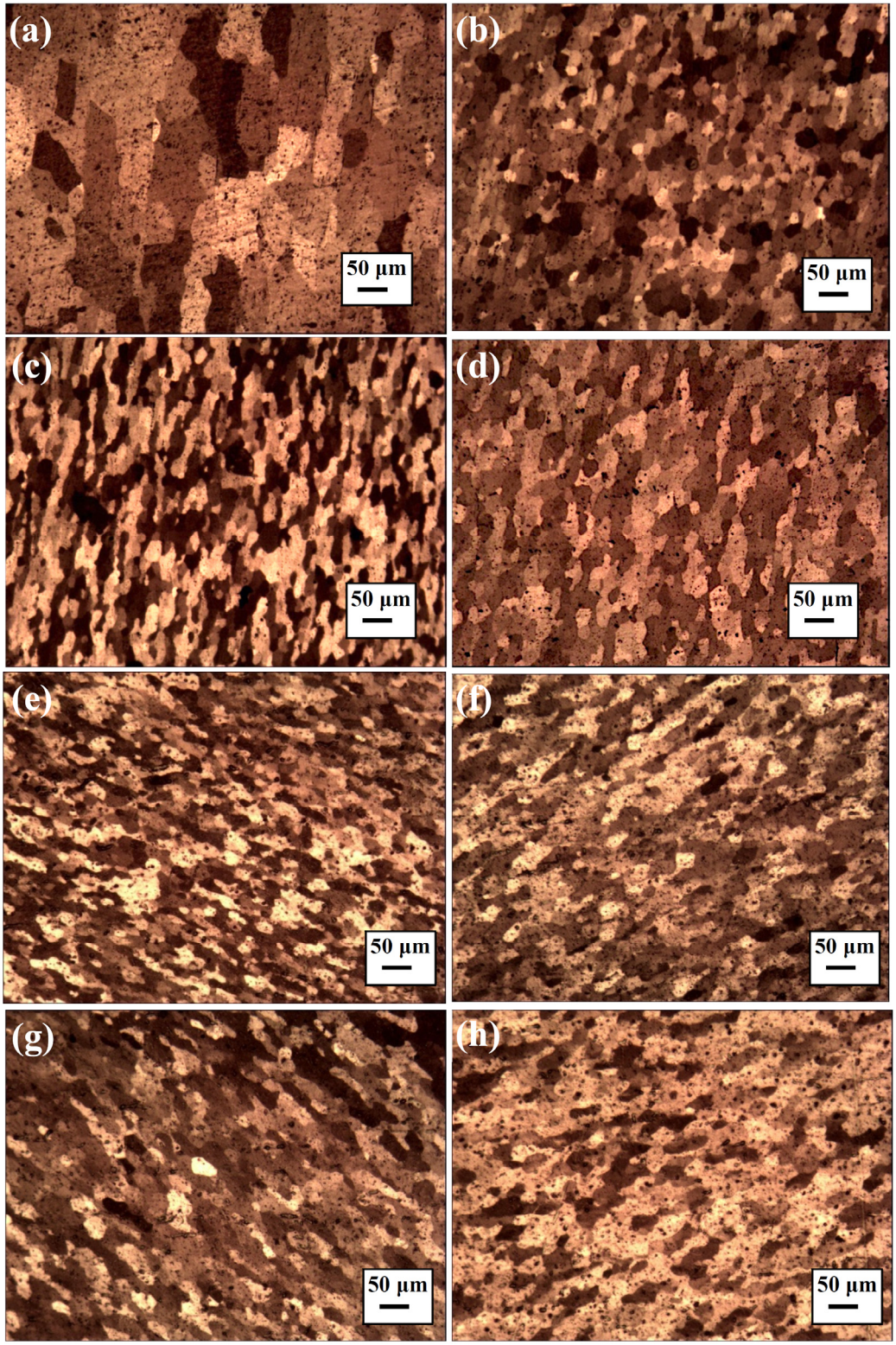

Fig. 3. Optical micrographs of (a) base, and threaded probe tool SZ of: (b) ω=800 rpm, ν=150 mm.min^{-1} (c) ω=1000 rpm, ν=50 mm.min^{-1}, (d) ω=1200 rpm, ν=150 mm.min^{-1}, (e) ω=1400 rpm, ν=200 mm.min^{-1}, (e) ω=1600 rpm, ν=100 mm.min^{-1}, (f) ω=1800 rpm, ν=100 mm.min^{-1} (g) ω=2000 rpm, ν=200 mm.min^{-1}.

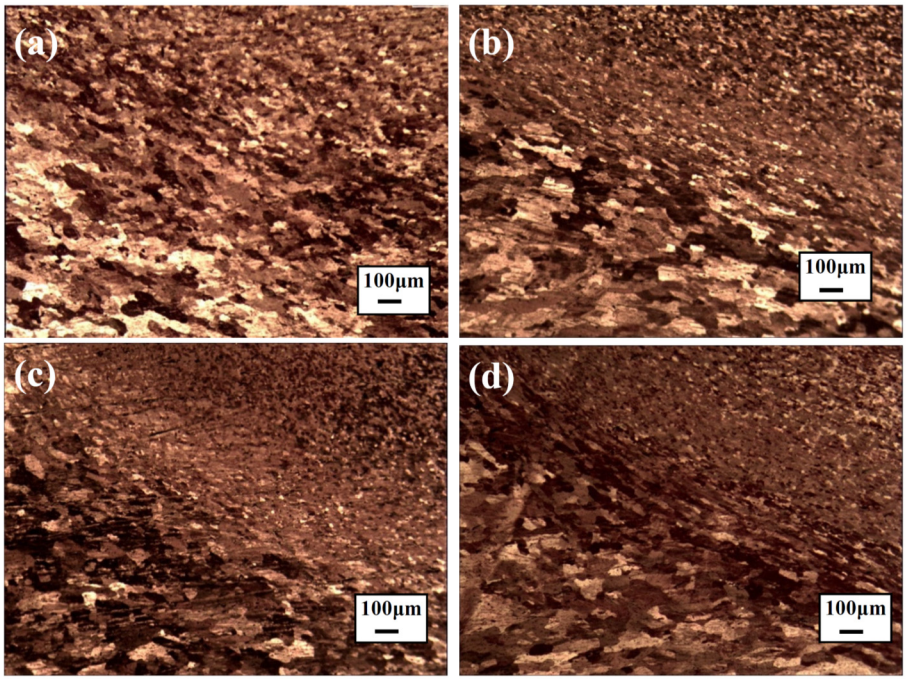

Fig. 4. SZ to BM micrograph of ω =1600 rpm, ν=100 mm.min^{-1} for different pin shape: (a) square, (b) triangular, (c) threaded, (d) columnar.

properties that make it suitable for specific kinds of materials [34]. By adding faces to the pin feature (triangular, square, and hexagonal), the pulse per second (pulses/sec = ω in seconds × number of flat faces) increases. The square probe produces 80 pulses per second, and the triangular produces 60 pulses per second for ν=100 mm.min^{-1} and ω =1600 rpm. The uniform flow of material produces a finer and homogeneous distribution of grains. Probe wear is a substantial drawback when using triangular and square pins, which adds the probe's material to the BM. The material's flow and the stir zone's size vary by changing the pin features. The depth, direction, and other thread characteristics also affect the SZ's flow and final microstructure [35].

3.3. Mechanical Properties

The average Vickers mean-hardness value of SZs for different ν-ω combinations processed with threaded probe pin is presented in Figure 5-a. As it is evident, increasing the heat input first enhances, and later on, decreases the stir zone's hardness. The Vickers mean-hardness value of the different probe shapes is presented in Figure 5-b, indicating that FSP increases hardness for all four tool probe shapes. Wear resistance also increases due to hardness enhancement by the threaded probe shape. It is evident that employing FSP stir the pasty material and break the grains; then, by DDRX, new distinctive, refined grains form with increased dislocation densities, where both thermo-mechanical and stirred zone's hardness were improved according to the Hall-Petch strengthening mechanism [36, 37]. The mean-hardness of initial annealed AA was 17, which improved to 28 Vickers (65% increase) after one FSP pass.

The UTS of different samples, including different ν, ω , and different probe shapes, are presented in Figure 6. Low YS with a limited strain hardening rate was observed for the tensile flow behavior of annealed AA1050 alloy. After FSP, all tensile properties were improved due to increased dislocation density, HAGB, and grain refinement [38, 39]. It is worth mentioning that the fraction of low angle and HAGB did not change too much; therefore, sharp UTS improvements were not observed [40, 41].

Comparing the tensile properties of samples show that the highest values were obtained in the threaded tool probe shape. UTS, YS, and El% were 49 MPa, 25 MPa, and 35 in BM, which changed to 81 MPa, 45 MPa, and 40 after one FSP pass (66%, 80%, and 14% enhancement, respectively).

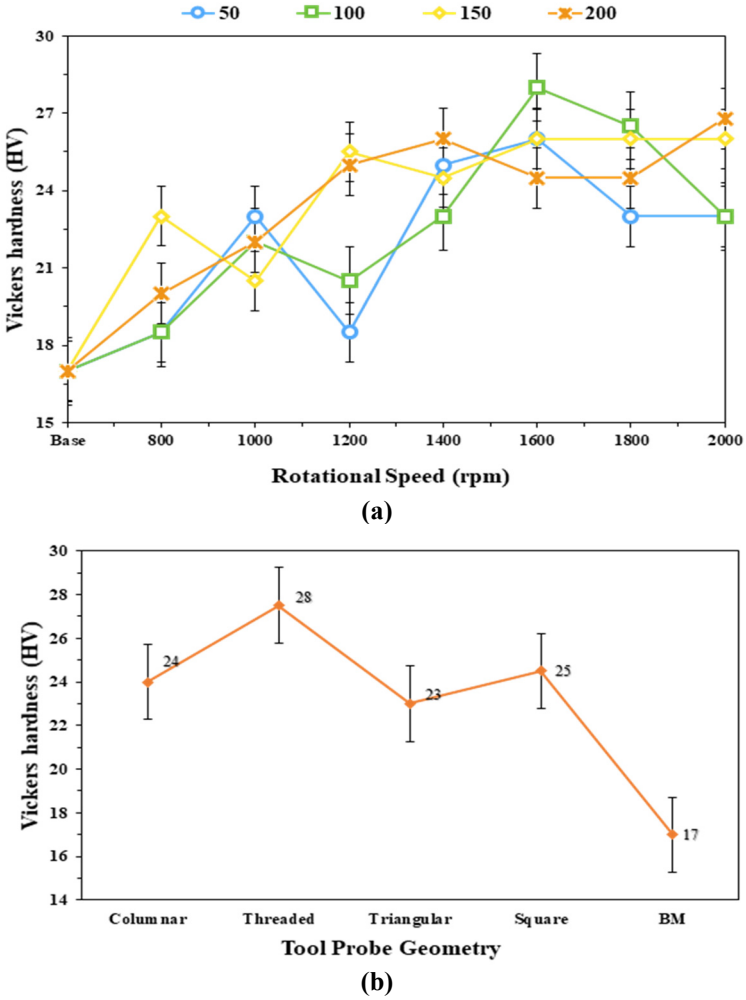

Fig. 5. The mean Vickers hardness value of SZs for (a) different ω -ν combinations, (b) different tool probe shape.

Overall, the improved mechanical properties of examined samples can be attributed to the increased dislocation density, which causes interaction between dislocations and grain boundaries, leading to grain boundary strengthening [24, 42, 43].

Figure 7 shows the OM and FESEM images, depicting fracture surfaces of the BM and processed specimen in a longitudinally tensile test. These images illustrate a fibrous dimple-like fracture mode with a negligible cleavage rupture around both samples' dimples. For the processed sample, the cleavage rupture portion is slightly more than BM because of the fine grains and higher strength. Dimples of both alloys are equiaxed, uniform, and homogeneous but are larger in BM. The elongated and finer dimples could be seen in the processed sample due to the finer grain structure [44]. The dimples in the BM are deeper than the processed sample since the nucleation of micro-voids and subsequent coalescence is influenced by the shear stress component, which leads to elongated dimples in the direction of the shear stresses [13].

4. CONCLUSIONS

In this research, the FSP parameters of ω =1600 rpm and ν=100 mm.min^{-1} along with using a threaded pin were identified as optimized choice for joining and modification of AA1050 based upon the grain refinement and tensile properties for FSP and FSW of AA1050. The SZ grain refinement occurred and the average grain size

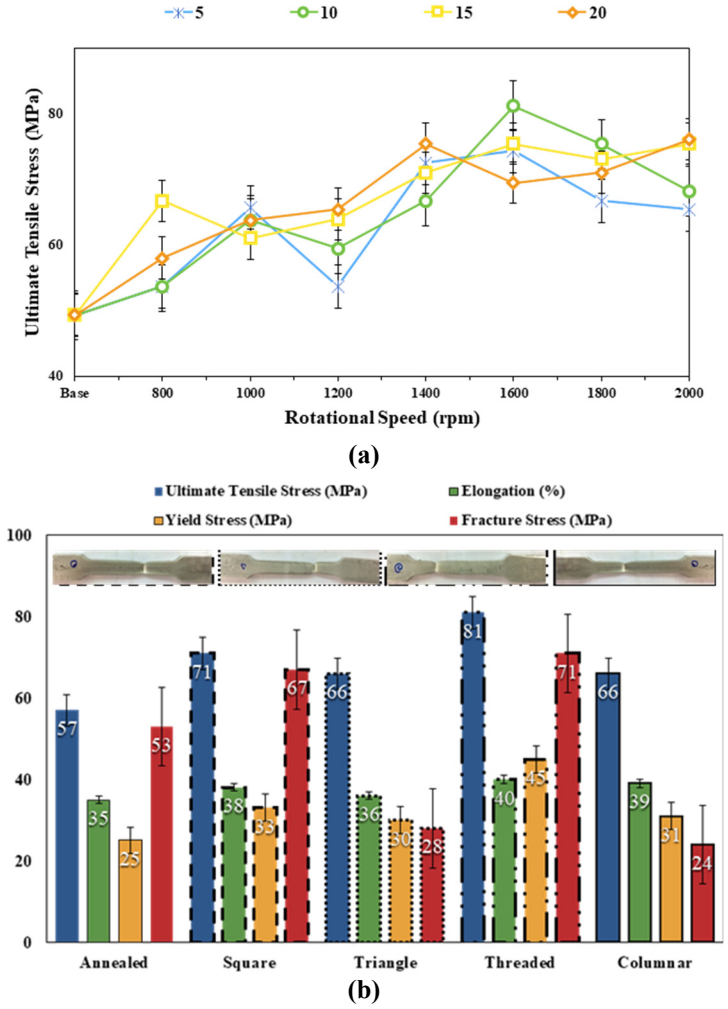

Fig. 6. Mechanical properties comparison: (a) UTS of 28 ω -v combinations, (b) different tool probe shapes.

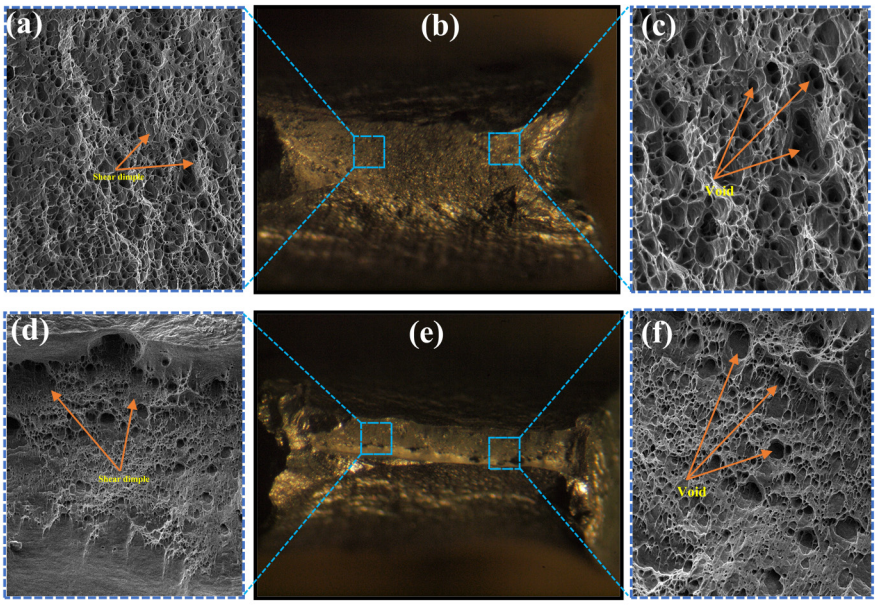

Fig. 7. OM & FESEM images showing the fracture surface of the tensile-tested specimens: (a,b,c) base alloy; (d,e,f) highest tensile properties sample (1600 rpm and 100 mm/min^{-1} with threaded probe shape).

was reduced from 30 down to 12 μm through DDRX. The indentation hardness of processed AA was increased by 68% to 28 Vickers due to the SZ's microstructural evolution. Also, significant improvement (80% YS, 66% UTS, and El% 14) and a satisfactory combination of all tensile properties (YS of 45 MPa, UTS of 81 MPa, and El% of 40) were attained for the processed AA as compared to the initial annealed AA (YS of 25 MPa, UTS of 49 MPa and El% of 35), along with a combined fracture behavior very close to the thoroughly ductile, with smaller and shallower holes than BM counterparts.

5. REFERENCE

[1] Sharma V, Prakash U, Kumar BVM. Surface composites by friction stir processing: A review. J. Mater. Process. Technol. 2015, 224, 117–134.

[2] Derazkola HA, Khodabakhshi F. A novel fed friction-stir (FFS) technology for nanocomposite joining. Sci. Technol. Weld. Join. 2019, 0,1–12.

[3] Mathers G. 8 - Other welding processes. In: Mathers G, editor. Weld. Alum. its Alloy. [Internet]. Woodhead Publishing; 2002. 147–165.

[4] Tang J, Shen Y, Li J. Influences of friction stir processing parameters on microstructure and mechanical properties of SiC/Al composites fabricated by multi-pin tool. J. Manuf. Process. 2019, 38,279–289.

[5] Węglowski MS. Friction stir processing – State of the art. Arch. Civ. Mech. Eng. 2018, 18,114–129.

[6] Kamikawa N, Hirochi T, Furuhara T. Strengthening Mechanisms in Ultrafine-Grained and Sub-grained High-Purity Aluminum. Metall. Mater. Trans. A Phys. Metall. Mater. Sci. 2019, 50,234–248.

[7] Avettand-Fènoël MN, Simar A. A review about Friction Stir Welding of metal matrix composites. Mater. Charact. 2016, 120,1–17.

[8] Ebadi M, Alishavandi M, Paydar MH. Anodizing behavior and electro-chemical evaluation of accumulative roll bonded Al and Al-SiC composite. Surf. Coatings Technol. 2021, 408:126776.

[9] Mishra RS, Ma ZY, Charit I. Friction stir processing: A novel technique for fabrication of surface composite. Mater. Sci. Eng. A. 2003, 341,307–310.

[10] Kwee I, De Waele W, Faes K. Weldability of high-strength aluminium alloy EN AW-7475-T761 sheets for aerospace applications, using refill friction stir spot welding. Weld. World. 2019, 63, 1001–1011.

[11] Gerlich AP. Critical assessment: friction stir processing, potential, and problems. Mater. Sci. Technol. 2017, 33, 1139–1144.

[12] Mousavizade SM, Pouranvari M, Malek Ghaini F, et al. Dynamic recrystallization phenomena during laser-assisted friction stir processing of a precipitation hardened nickel base superalloy. J. Alloys Compd. 2016, 685,806–811.

[13] Alishavandi M, Ebadi M, Alishavandi S, et al. Microstructural and mechanical characteristics of AA1050/mischmetal oxide in-situ hybrid surface nanocomposite by multi-pass friction stir processing. Surf. Coatings Technol. 2020, 388:125488.

[14] Doherty RD, Hughes DA, Humphreys FJ, et al. Current issues in recrystallization: A review. Mater. Sci. Eng. A. 1997, 238,219–274.

[15] Du B, Yang X, Liu K, et al. Effects of supporting plate hole and welding force on weld formation and mechanical property of friction plug joints for AA2219-T87 friction stir welds. Weld. World. 2019, 63,989–1000.

[16] Deore HA, Mishra J, Rao AG, et al. Effect of filler material and post process ageing treatment on micro-structure, mechanical properties and wear behaviour of friction stir processed

AA 7075 surface composites. Surf. Coatings Technol. 2019, 374, 52–64.
[17] Han J, Chen J, Peng L, et al. Microstructure, texture and mechanical properties of friction stir processed Mg-14Gd alloys. Mater. Des. Elsevier Ltd; 2017.
[18] Rafiei R, Ostovari Moghaddam A, Hatami MR, et al. Microstructural characteristics and mechanical properties of the dissimilar friction-stir butt welds between an Al–Mg alloy and A316L stainless steel. Int. J. Adv. Manuf. Technol. 2017, 90, 2785–2801.
[19] Huang K, Logé RE. A review of dynamic recrystallization phenomena in metallic materials. Mater. Des. 2016; 111,548–574.
[20] Eslami N, Harms A, Henke B, et al. Electrical and mechanical properties of friction stir welded Al-Cu butt joints. Weld. World. 2019, 63,903–911.
[21] Eskandari H, Taheri R, Khodabakhshi F. Friction-stir processing of an AA8026-TiB_2-Al_2O_3 hybrid nano-composite: Microstructural develop-ments and mechanical properties. Mater. Sci. Eng. A. 2016, 660, 84–96.
[22] Sarkari Khorrami M, Kazeminezhad M, Miyashita Y, et al. The Correlation of Stir Zone Texture Development with Base Metal Texture and Tool-Induced Deformation in Friction Stir Processing of Severely Deformed Aluminum. Metall. Mater. Trans. A Phys. Metall. Mater. Sci. 2017, 48,188–197.
[23] McQueen HJ, Solberg JK, Ryum N, et al. Evolution of flow stress in aluminium during ultra-high straining at elevated temperatures. Part II. Philos. Mag. A Phys. Condens. Matter, Struct. Defects Mech. Prop. 1989, 60,473–485.
[24] Khodabakhshi F, Simchi A, Kokabi AH, et al. Influence of hard inclusions on microstructural characteristics and textural components during dissimilar friction-stir welding of an PM Al–Al_2O_3–SiC hybrid nanocomposite with AA1050 alloy. Sci. Technol. Weld. Join. 2017. 412–427.
[25] Mahmoud TS, Shaban OM, Zakaria HM, et al. On effect of FSP on microstructural and mechanical characteristics of A390 hypereutectic Al – Si alloy. 2010, 26, 2–6.
[26] Pasebani S, Charit I, Mishra RS. Effect of tool rotation rate on constituent particles in a friction stir processed 2024Al alloy. Mater. Lett. 2015, 160, 64–67.
[27] Vignesh RV, Padmanaban R, Datta M. Influence of FSP on the microstructure, microhardness, intergranular corrosion susceptibility and wear resistance of AA5083 alloy. Tribol. - Mater. Surfaces Interfaces. 2018, 12,157–169.
[28] R.S. Mishra, Z.Y. Ma. Friction Stir Welding and Processing II Article in Materials Science and Engineering R Reports September 2005. Mater. Sci. Eng. R. 2014, 50, 1–78.
[29] Patel V V., Badheka V, Kumar A. Friction Stir Processing as a Novel Technique to Achieve Superplasticity in Aluminum Alloys: Process Variables, Variants, and Applications. Metallogr. Microstruct. Anal. 2016, 5,278–293.
[30] Liu J, Wang X, Liu J, et al. Hot deformation and dynamic recrystallize-tion behavior of Cu-3Ti-3Ni-0.5Si alloy. J. Alloys Compd. 2019; 782, 224–234.
[31] Alishavandi M, Razmjoo Khollari MA, Ebadi M, et al. Corrosion-wear behavior of AA1050 / mischmetal oxides surface nanocomposite fabricated by friction stir processing. J. Alloys Compd. 2020, 832,153964.
[32] Sharma DK, Badheka VJ, Patel V, et al. Recent developments in hybrid surface metal matrix composites produced by friction stir processing: A review. J. Tribol. 2021, 1–58.

[33] Alishavandi M, Mohammadmirzaei M, Ebadi M, et al. Microstructural and mechanical evaluation of submerged arc welded HSLA 4135 steel by modeled and manufactured granular Cr-Mo bonded active basic flux. J. Mater. Process. Technol. 2020, 116890.
[34] Mosavvar A, Azdast T, Moradian M, et al. Tensile properties of friction stir welding of thermoplastic pipes based on a novel designed mechanism. Weld. World. 2019, 63,691–699.
[35] Alvand M, Naseri M, Borhani E, et al. Microstructure and Crystallographic Texture Characterization of Friction Stir Welded Thin AA2024 Aluminum Alloy. Iran. J. Mater. Sci. Eng. 2018, 15.
[36] Demouche M, Ouakdi EH, Louahdi R. Effect of Welding Parameters in the Microstructure and Mechanical Properties of Friction-Welded Joints of 100Cr6 Steel. Iran. J. Mater. Sci. Eng. 2019, 16:24–31.
[37] Zamani MH, Divandari M, Tamizifar M. On the Characteristics of Friction Stir Welding Lap Joint of Magnesium and Aluminum. Iran. J. Mater. Sci. Eng. 2018, 15, 64–77.
[38] Khodabakhshi F, Gerlich AP, Švec P. Fabrication of a high strength ultra-fine grained Al-Mg-SiC nanocomposite by multi-step friction-stir processing. Mater. Sci. Eng. A. 2017, 698, 313–325.
[39] Su JQ, Nelson TW, Sterling CJ. Grain refinement of aluminum alloys by friction stir processing. Philos. Mag. 2006, 86, 1–24.
[40] Nene SS, Liu K, Frank M, et al. Enhanced strength and ductility in a friction stir processing engineered dual phase high entropy alloy. Sci. Rep. 2017, 7, 1–7.
[41] Sarkari Khorrami M, Kazeminezhad M, Kokabi AH. Thermal stability during annealing of friction stir welded aluminum sheet produced by constrained groove pressing. Mater. Des. 2013, 45, 222–227.
[42] Dinaharan I, Murugan N. Optimization of friction stir welding process to maximize tensile strength of AA6061/ZrB_2 in-situ composite butt joints. Met. Mater. Int. 2012, 18,135–142.
[43] Jayaraman M, Sivasubramanian R, Balasubramanian V, et al. Influences of process parameters on tensile strength of friction stir welded cast A319 aluminium alloy joints. Met. Mater. Int. 2009, 15,313–320.
[44] Khodabakhshi F, Simchi A, Kokabi AH, et al. Reactive friction stir processing of AA 5052-TiO_2 nanocomposite: Process - microstructure - mechanical characteristics. Mater. Sci. Technol. 2015, 31,426–435.